A Multivortex Method for Axisymmetric Bodies at Angle of Attack

SILVIO B. ANGELUCCI*
McDonnell Douglas Astronautics Company, Huntington Beach, Calif.

A multivortex model made up of a large number of discrete free vortices has been used to represent the actual vortex sheets shed from the lee side of a slender body at an angle of attack. Circulation, strength, and position of the vortices, together with the induced normal forces, are evaluated at various axial positions along the body axis. The viscous inputs to the analysis are the separation or feeding points which are provided by experiment or semi-empirical theories. A discussion of the numerical computations and a comparison with experimental data are presented.

Nomenclature

x,y,z = body axes
a = $d/2$ = base or reference radius
C_N = $N/(0.5\rho_\infty V_\infty^2 \pi a^2)$ = normal force coefficient
C_m = $M/(\rho_\infty V_\infty^2 \pi a^3)$ = pitching moment coefficient
$C_{N\alpha}$ = $(\partial C_N/\partial\alpha)_{\alpha=0}$
$C_{m\alpha}$ = $(\partial C_m/\partial\alpha)_{\alpha=0}$
C_{Nv}, C_{mv} = vortex induced normal force and pitching moment coefficients
C_{Nx} = dC_{Nv}/dx = local normal force coefficient
C_{Dc} = $D/(\rho_\infty V_\infty^2 \sin^2\alpha a)$ = cross-flow drag coefficient
I = total impulse
l = body total length
M = Mach number
n = number of vortices
Re = Reynolds number
r_0 = body local radius
$\bar{r}_A$ = nondimensional length of the vortex sheet
s = length measured along the vortex sheet from point of separation
t = time
V_∞ = freestream velocity
w = $u + iv$ = complex velocity in the cross-flow plane
u',v',w' = nondimensional velocities, $u' = u/V_\infty \ldots$
α = angle of attack
β = relative incidence, $\beta = \tan\alpha/\tan\epsilon$
γ = circulation per unit length of the vortex sheet
Γ = circulation strength of vortex sheet or discrete vortex
ϵ = semiapex angle of the cone
λ = $\Gamma/2\pi V_\infty r_0$ = nondimensional circulation strength, also $\lambda' = \lambda r_0/a$
ρ = air density
σ = $\xi + i\eta$; $\bar{\sigma} = \xi - i\eta$ = complex coordinate, also $\sigma = re^{i\theta}$; $\bar{\sigma} = re^{-i\theta}$
Φ = $\phi + i\psi$ = complex velocity potential (or potential function)
ϕ = velocity potential
ϕ^* = angular orientation of the vortex sheet at the center of vorticity
ϕ_s = angular orientation of the vortex sheet at the separation point
ψ = stream function
$|\ |$ = absolute value of
conj [ ] = conjugate of [ ]
$IP\{\ \}$; $RP\{\ \}$ = imaginary part of { }; real part of { }

Subscripts

$(\ )_s$ = evaluated at the separation point S
$(\ )_i$ = evaluated at the generic point i at the vortex sheet
$(\ )_j$ = evaluated at the generic point j in the σ plane
$(\ )_{th}$; $(\ )_{exp}$ = theoretical and experimental value

1. Introduction

THE aerodynamic characteristics of supersonic airplanes, missiles, submarines, and other slender lifting bodies operating at high angles of attack can be profoundly influenced by the presence of vortices separating from the vehicle fuselage. A large nonlinear increase of normal force with increasing angle of attack, together with a rearward shift of the center of pressure, can be produced by vortex separation; predominant effects are experienced at subsonic and low supersonic speeds. Furthermore, the effectiveness of aft control surfaces or fins can be greatly reduced by the vortex wake produced by forward separation.

The flow separates from the body surface along a three-dimensional separation line; that is, where the primary boundary layer no longer can penetrate the adverse pressure gradient, and rolls up into a region of concentrated circulation assuming the characteristic form of vortex sheet spirals as shown in Fig. 1a. Experimental observations conducted on various slender configurations[1-3] have indicated that the vortex separation is basically a cross-flow type of separation and that its effect on the aerodynamic characteristics of slender bodies can be, in general, analyzed by an inviscid model based on the approximations of slender body theory.

The first significant step in representing the actual vortex sheet spirals by an inviscid mathematical model was presented by Edwards[4] and Brown and Michael[5] in the problem of a slender delta wing exhibiting leading-edge separation. The model consists of two symmetrical concentrated vortices connected to the separation points by two feeding sheets of vanishing strength at the wing surface. Bryson[6] used this model to obtain a solution for the nonlinear forces on circular cones and cylinders; the two vortex model has been later extended to apply to bodies of elliptic cross section and of cambered longitudinal axis.[7,8]

This model neglects the contribution of the feeding sheet to the separation condition and, except for the case of the cylin-

Received November 11, 1970; revision received June 4, 1971. This work was prepared under the sponsorship of the McDonnell Douglas Astronautics Company Independent Research and Development Program. The author is indebted to A. I. Ormsbee for his interest and suggestions and to K. Pennington Jr., and W. A. Anderson for their computational assistance.

Index categories: Launch Vehicle and Missile Configurational Design; Subsonic and Transonic Flow.

* Senior Engineer/Scientist, Aero/Thermodynamics and Nuclear Effects. Member AIAA.

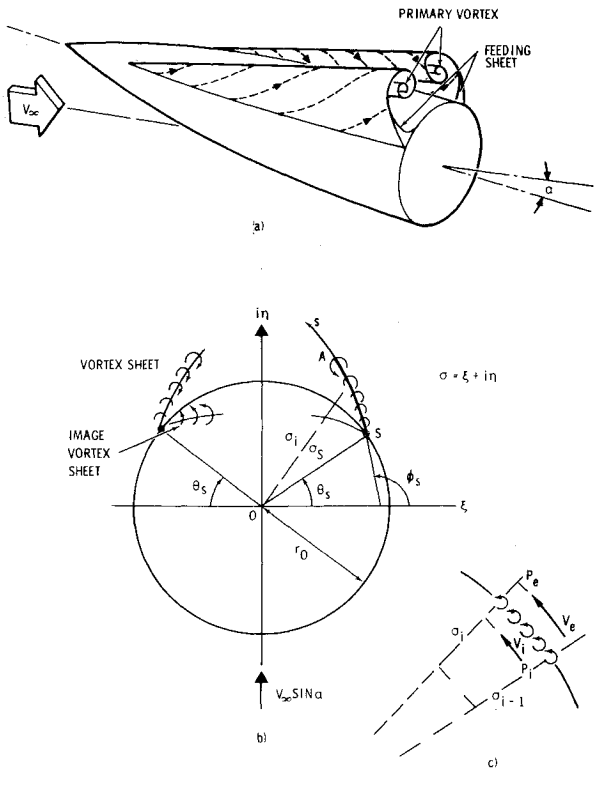

Fig. 1 Vortex separation on a 3-D body and mathematical model.

der, takes advantage of the conical nature of the flowfield; the condition that no net force is substained by the concentrated vortex and its feeding sheet is also assumed.

A more realistic model that accounts for finite vorticity in the feeding sheets was considered by Mangler and Smith[9] in 1957 in their slender delta wing theory. Each vortex spiral is regarded as consisting of two parts: an inner part which is replaced by an isolated potential vortex and an outer part represented by a vortex sheet lying along an analytical curve, which is defined in a convenient transformed plane by imposing the continuity of pressure and zero normal velocity conditions. The flow is still conical and lengthy computations and personal judgment were required to solve the governing equations.

An alternative way to approximate the outer part of the vortex sheet was proposed by Smith[10] who used a large number of small concentrated vortices at arbitrarily chosen points on it. This approach allows the solution of the transcendental equations of Mangler and Smith by using a finite difference technique. Theoretically, the model can be improved to any desired accuracy by increasing the number of vortices.

Finally, Sacks et al.[11] have suggested a delta wing theory in which the entire vortex sheets shed from the wing leading edges are represented by a finite number of vortex sheet segments. These segments are then replaced by concentrated vortices whose subsequent positions are computed step-by-step from the local induced velocities at the vortices. This model allows the vortex sheets to roll up freely without the restriction of concentrated vortex cores and does not rely on the assumptions of conical flow.

The improvements obtained in the wing problem with mathematical models that gave adequate considerations to the feeding sheet have stimulated the present study. The intent of this paper is to present an analytical method based on inviscid theory that is capable of evaluating the vortex induced forces on slender axisymmetric bodies exhibiting symmetrical separation. The mathematical model takes into account the vorticity in the feeding sheet and does not have the restriction of conical flow. This model is similar to the one used by Sacks et al.[11] in the wing problem but differs substantially in the mathematical definition of the elementary vortex sheet (labeled "line filament" in Ref. 11). In fact, the vorticity distribution and the orientation of the elementary vortex sheets are not taken as a constant as in Ref. 11, but are determined from the conditions of no normal pressure force and zero normal velocity at the sheet itself.

The separation line, which in the wing problem is known "a priori," being fixed at the wing leading edge, is implemented here, as in Bryson[6] and other models,[7,8] by empirical data or approximate theories. The present model can also be extended to include bodies of asymmetrical cross-sectional shapes.

2. General Assumptions

In accordance with most of the theoretical investigations[6,7,11] the approach to the present problem is to assume that the attached flow and separated flow characteristics are separable and additive. The total normal force or moment will be the sum of the linear force due to the attached flow and of the nonlinear force induced by vortex separation

$$C_N = C_{N_\alpha}\alpha + C_{N_v} \tag{1}$$

The effects of vortex separation over three-dimensional slender lifting bodies can be analyzed by approximating the actual flow by an analogous time-varying two-dimensional flow.[12] The linearized equation for the velocity potential of a two-dimensional time-varying incompressible flow becomes

$$\partial^2\phi/\partial y^2 + \partial^2\phi/\partial z^2 = 0 \tag{2}$$

when the change in shape of the body is accounted for in the form of a time-dependent boundary condition.

It is assumed that the freestream conditions and the body geometry are such that only symmetrical separation occurs on the body surface. The feeding points, which represent the viscous input to the analysis, are provided by experiment or semiempirical theories.

3. Flow Representation

The actual leeward vortex sheets of a slender body at an angle of attack are approximated by a finite number of discrete elementary vortex sheets. In particular, each elementary vortex sheet pair represents the vorticity shed by the body surface during a time interval Δt. If the time interval, Δt, is replaced by $\Delta x/V_\infty \cos\alpha$, each pair of elementary vortex sheets is shed at each of a finite number of corresponding axial positions. The vortex sheet pair is then replaced by a pair of equivalent concentrated vortices. These vortices are treated as free vortices of constant strength and their subsequent positions are computed step-by-step from the total velocity induced at the vortices. The normal force distribution along the body is computed from the strength and position of the discrete vortices at each axial station.

4. Analysis

Within the assumptions previously discussed, the Laplace equation has to be solved at each body cross section. Consider a generic cross section, x = const, of an axisymmetric body represented by a circle of radius r_0 in the complex plane $\sigma = \xi + i\eta$ of Fig. 1. An axisymmetric body with continuous and monotonic variation of radius is equivalent to an expanding (or contracting) circular cylinder. The complex velocity potential representing the flow about this expanding cylinder immersed in a vertical crossflow stream of velocity $V_\infty \sin\alpha$ is

$$\Phi_1(\sigma) = c\,ln\,\sigma - iV_\infty \sin\alpha(\sigma - r_0^2/\sigma) \tag{3}$$

where $\Phi(\sigma) = \phi(\sigma) + i\psi(\sigma)$, $\phi(\sigma)$ being a solution of the Laplace equation and $\psi(\sigma)$ the stream function.

Suppose that the boundary layer leaves the body surface at the points of separations σ_s and $-\bar{\sigma}_s$ in the form of a curved vortex sheet growing, in the time interval Δt and along the curvilinear coordinate s, from $s = 0$, $(\sigma = \sigma_s)$, to $s = s_A$, $(\sigma = \sigma_A)$. If $\gamma(s)$ represents the vorticity or circulation per unit length of the vortex sheet, then the complex velocity potential of a pair of vortex sheets of opposite strength can be expressed in the form

$$\Phi_2(\sigma) = -\frac{i}{2\pi}\int_0^{s_A} \gamma(s) ds \ln \frac{(\sigma - \sigma_i)(\sigma + r_0^2/\sigma_i)}{(\sigma + \bar{\sigma}_i)(\sigma - r_0^2/\bar{\sigma}_i)} \quad (4)$$

where $\phi(\sigma) = RP[\Phi(\sigma)]$ still represents a solution of Eq. (2). To preserve the boundary condition of no cross-flow at the body surface, two image vortex sheets have been included in the potential function $\Phi_2(\sigma)$. A solution of the type expressed by Eq. (4) is required at each of a finite number of axial positions where vortex sheets are supposed to be shed by the body surface.

At the body axial station $x = x_s$, where the vortex separation first starts, the total complex velocity potential is made up of the sum of Eqs. (3) and (4). At the generic axial station, $x_n = x_s + n\Delta t/V_\infty \cos\alpha$,

$$\Phi(\sigma) = c\ln\sigma - iV_\infty \sin\alpha\left(\sigma - \frac{r_0^2}{\sigma}\right) - \frac{i}{2\pi}\int_0^{s_A} \gamma(s)\, ds \ln \frac{(\sigma - \sigma_i)(\sigma + r_0^2/\sigma_i)}{(\sigma + \bar{\sigma}_i)(\sigma - r_0^2/\bar{\sigma}_i)} - \frac{i}{2\pi}\sum_{j=1}^{n-1} \Gamma_j \ln \frac{(\sigma - \sigma_j)(\sigma + r_0^2/\sigma_j)}{(\sigma + \bar{\sigma}_j)(\sigma - r_0^2/\bar{\sigma}_j)} \quad (5)$$

The third term of Eq. (5) represents now the contribution of the vorticity shed between the axial stations, x_{n-1} and x_n. The last term is the contribution of the $(n-1)$ elementary vortex sheets shed at the upstream station x_j, $(j = 1, 2, \ldots n-1)$; for reasons of mathematical simplicity they have been replaced by equivalent concentrated vortices of strength Γ_j.

The velocity at any point σ of the field is determined by differentiating the complex velocity potential

$$w = u + iv = \mathrm{conj}[d\Phi(\sigma)/d\sigma] \quad (6)$$

where the real and imaginary parts of the complex velocity represent, respectively, the total velocity components along the ξ and η axes.

The solution of the problem requires first the definition of a Kutta type separation condition at the feeding points. In the present case, this condition states that the total fluid velocity relative to the body is zero at the feeding points; that is, these points are stagnation points

$$w = 0 \quad \text{at} \quad \sigma = \sigma_s \quad (7)$$

The separation condition has to be satisfied every time a new pair of elementary vortex sheets is introduced. It has to be noticed that the source term for a growing body radius will not contribute to the condition expressed by Eq. (7), since it vanishes at the body surface.

The other conditions necessary to completely define the present problem depend on the definition of vortex sheet and on the assumed separation mechanism. By definition, a vortex sheet is a surface of discontinuity dividing two regimes of flow. Consider the boundary between two potential flows with a velocity discontinuity, as in Fig. 1c. If ds represents a short length of the section of the boundary, the circulation or total vortex strength of ds is equal to $(v_e - v_i)ds = \gamma ds$. The total head on either side of the boundary is

$$H_e = p_e + \tfrac{1}{2}\rho v_e^2; \qquad H_i = p_i + \tfrac{1}{2}\rho v_i^2 \quad (8)$$

Letting $v_b = (\frac{1}{2})(v_e + v_i)$, the average velocity in the boundary, the pressure difference between the two regions of flow can be expressed in the form[13]

$$\Delta p = \rho v_b \gamma + \Delta H \quad (9)$$

If the total head on either sides differs by the amount $\rho v_b \gamma$, a free boundary can be formed which takes no normal pressure force. The general trend of the flow separation from the lee side of slender cones seems to confirm the existence of such a free boundary; this is also the case of rear separation from a wing profile as pointed out by Kuchemann.[13] If a free boundary exists at least during the incipient separation, then the vorticity distribution and the orientation of the vortex sheet can be determined from the conditions that the boundary is a streamline and that the pressure across it is continuous. These conditions can be approximately satisfied by imposing that: a) the vortex sheet is oriented in the direction of the total velocity vector induced at a specified point of the sheet, nominally the "center of vorticity," and b) the vorticity distribution is such that the average velocity normal to the sheet and induced by the sheet itself is zero. The "center of vorticity" is defined as the point of the vortex sheet where the total strength can be concentrated in order to induce at the generic point σ the same total velocity as the vortex sheet.

If ϕ^* represents the orientation of the vortex sheet at the center of vorticity σ^*, the condition a) can be expressed in the form

$$RP\{[w]_{\sigma=\sigma^*}\} \sin\phi^* + IP\{[w]_{\sigma=\sigma^*}\} \cos\phi^* = 0 \quad (10)$$

The simplest vorticity distribution that satisfies the condition b) and that gives no singular downwash at the edges of the sheet is of the form

$$\gamma(s) = k|\sigma_A - \sigma_i||\sigma_i - \sigma_s| \quad (11)$$

where k is a constant and σ_i, $\sigma_s \leq \sigma_i \leq \sigma_A$, is the generic point on the vortex sheet.

It has been observed in experiments on circular cones that during vortex separation, the general conical nature of the flowfield is preserved. This flowfield trend allows the definitions of the last unknown of the problem, that is, the length $\int_s ds$ of the elementary vortex sheet in each cross-flow plane. It is assumed that the extent of the vortex sheet increases linearly with the step size Δt or $\Delta x (= V_\infty \cos\alpha \Delta t)$ and that it can be approximated by a straight segment line. This is always possible when the step size is kept sufficiently small. The vorticity distribution then becomes

$$\gamma(s) = k(\sigma_A - \sigma_i)(\sigma_i - \sigma_s)e^{-i2\phi_s} \quad (12)$$

where ϕ_s represents the orientation with respect to the real axis ξ, of the segment line leaving the surface at σ_s.

Kutta Condition

With the use of Eq. (12) the Kutta condition can now be expressed in the form

$$\mathrm{conj}\left\{-iV_\infty \sin\alpha\left[1 + \frac{r_0^2}{\sigma_s^2}\right] - \frac{i}{2\pi}\sum_j^{n-1} \Gamma_j \times \left[\frac{1}{\sigma_s - \sigma_j} + \frac{1}{\sigma_s + (r_0^2/\sigma_j)} - \frac{1}{\sigma_s + \bar{\sigma}_j} - \frac{1}{\sigma_s - r_0^2/\bar{\sigma}_j}\right] - \frac{ike^{-i3\phi_s}}{2\pi}\int_{\sigma_s}^{\sigma_A} (\sigma_A - \sigma_i)(\sigma_i - \sigma_s)\left[\frac{1}{\sigma_s - \sigma_i} + \frac{1}{\sigma_s + (r_0^2/\sigma_i)} - \frac{1}{\sigma_s + \bar{\sigma}_i} - \frac{1}{\sigma_s - r_0^2/\bar{\sigma}_i}\right] d\sigma_i\right\} = 0 \quad (13)$$

This condition has to be satisfied at each axial station x_i that is, every time a new elementary vortex sheet is introduced. Equation (13) gives the strength of the newly shed vortex sheet as a function of its length and orientation.

If $\bar{r}_A$ indicates the nondimensional length of the elementary vortex sheet, such that

$$\sigma_A - \sigma_s = \bar{r}_A r_0 e^{i\phi_s} \tag{14}$$

Equation (13) becomes, after some algebra[14]

$$\frac{k\bar{r}_A^2 r_0^2}{4\pi V_\infty}\left[2\cos(\phi_s-\theta_s)+\frac{1}{3}\bar{r}_A-\sum_{p=1}^{\infty}\frac{4}{(p+2)(p+3)}\times\left(-\frac{\bar{r}_A}{2}\right)^{p+1}\frac{\cos(p\phi_s-\theta_s)}{\cos^{p+1}\theta_s}\right]=2\sin\alpha\cos\theta_s-\sum_{j=1}^{n-1}\lambda_j(r_j^2-r_0^2)\left(\frac{1}{r_{js}^2}-\frac{1}{\bar{r}_{js}^2}\right) \tag{15}$$

where

$$r_j=|\sigma_j| \qquad r_{js}=|\sigma_j-\sigma_s| \qquad \bar{r}_{js}^2=r_{js}^2+4\xi_j\xi_s \tag{16}$$

and where $\lambda = (\Gamma/2\pi V_\infty r_0)$ represents the nondimensional strength of the discrete vortex previously shed, with

$$\Gamma = e^{-i\phi_s}\int_{\sigma_s}^{\sigma_A}\gamma(s)d\sigma = \frac{1}{6}k\bar{r}_A^3 r_0^3 \tag{17}$$

The last term of the right side of Eq. (15), that is, the absolute value of the velocity induced by the discrete vortices will be later identified simply by

$$\left|\sum_{j=1}^{n-1} w_j'\right|$$

Vortex Sheet Orientation

The orientation of the elementary vortex sheet at the beginning of separation is evaluated by solving Eq. (10) for σ^* approaching σ_s. If Γ, $\frac{1}{6}k\bar{r}_A^3 r_0^3$, represents the total circulation of the vortex sheet, using the aforementioned definition of vortex sheet one obtains

$$e^{-i\phi_s}\int_{\sigma_s}^{\sigma_A}\frac{\gamma d\sigma_i}{\sigma_s-\sigma_i}=\frac{\Gamma}{\sigma_s-\sigma^*} \tag{18}$$

which, solved with respect to σ^*, yields $\sigma^* = \sigma_0 + \frac{1}{3}\bar{r}_A r_0 e^{i\phi_s}$.

It is interesting to note that, with an elliptic distribution of circulation, the center of vorticity is placed at one third of the sheet length. The velocity induced at σ^* by the vortex sheet system can be approximated by

$$w_{vs}' = \mathrm{conj}\left[-\frac{i}{2\pi V_\infty}\frac{k}{6}\bar{r}_A^3 r_0^3\times\left(\frac{1}{\sigma^*+r_0^2/\sigma^*}-\frac{1}{\sigma^*+\bar{\sigma}^*}-\frac{1}{\sigma^*-r_0^2/\bar{\sigma}^*}\right)\right] \tag{19}$$

where the left side vortex sheet and the two image vortex sheets (into the circle of radius r_0) have been replaced by concentrated vortices at their center of vorticity. The contribution of the right side vortex sheet in the Eq. (19) is zero by definition.

If in Eq. (19) σ^* is replaced by $\sigma_0 + [\Delta\sigma, \Delta\sigma = (\frac{1}{3})\bar{r}_A r_0 e^{i\phi_s}]$, and the resulting expression is expanded in series of $\Delta\sigma$, the Eq. (19) with the use of Eq. (15) becomes, as σ^* approaches σ_0

$$w_{vs}' \cong \left[\left(2\sin\alpha\cos\theta_s-\left|\sum_{j=1}^{n-1}w_j'\right|\right)\Big/4\cos^2(\phi_s-\theta_s)\right]\times(\sin\theta_s - i\cos\theta_s) \tag{20}$$

Operating in similar manner with the velocities induced by the cross-flow, growing body and vortices already shed, the Eq. (10) becomes after some algebra[14]

$$\tan^2(\phi_s-\theta_s)+\left[4\frac{dr_0}{dx}\Big/\left(2\sin\alpha\cos\theta_s-\left|\sum_{j=1}^{n-1}w_j'\right|\right)\right]\times\tan(\phi_s-\theta_s)-3=0 \tag{21}$$

The orientation of the vortex sheet at each axial station is then obtained by solving Eq. (21) and disregarding the unstable root. If w_n represents the velocity component normal to the vortex sheet, the condition to be satisfied by the stable root is $\partial w_n/\partial\sigma_s > 0$, that is

$$\tan(\phi_s-\theta_s)+\left[2\frac{dr_0}{dx}\cos^2(\phi_s-\theta_s)\Big/\left(2\sin\alpha\cos\theta_s-\left|\sum_{j=1}^{n-1}w_j'\right|\right)\right]>0 \tag{22}$$

For both a cylinder and an axisymmetric body with increasing radius this condition simply becomes $\theta_s < \phi_s \leq \theta_s + \pi/2$. For an axisymmetric body with increasing radius the orientation of the vortex sheet changes with the axial station, whereas for a cylinder it is always $\phi_s = \theta_s + \pi/3$. This orientation is identical to the value obtained by Bryson[6] for the orientation of his feeding sheet.

Vortex Sheet Length

It has been assumed that the extent of the vortex sheet increase, linearly with the step size and that it can be approximated by a straight line. The length of the vortex sheet can be evaluated, in the same vein as the orientation but with an alternative approximation, from the component along the vortex sheet of the total velocity induced at the center of vorticity, which is made to approach the separation point by a limiting process. In a first approximation it is,

$$\bar{r}_A = \left\{\frac{dr_0}{dx}\cos(\phi_s-\theta_s)+\left(2\sin\alpha\cos\theta_s-\left|\sum_{j=1}^{n-1}w_j'\right|\right)\sin(\phi_s-\theta_s)\right\}\frac{\Delta x}{r_0} \tag{23}$$

Vortex Sheet Development and Trajectory

Once the elementary vortex sheet pair is completely defined at the generic axial station x_n, then a pair of equivalent discrete vortices is introduced. The strength, Γ_n, $-\Gamma_n$, is given by Eq. (17) and the position σ_n, $-\bar{\sigma}_n$, is computed by imposing the same Kutta condition already satisfied by the vortex sheet pair. If the left side of Eq. (15) is replaced by

$$(\Gamma_n/2\pi V_\infty r_0)(r_n^2 - r_0^2)(1/r_{n0}^2 - 1/\bar{r}_{n0}^2) \tag{24}$$

and the assumption is made that the discrete vortex lies somewhere along the vortex sheet, then Eq. (15) becomes after some algebra

$$\eta_n^3+\left(\frac{e-1}{ce}-3\eta_s\right)\eta_n^2+\left[3\eta_s^2+\frac{d(e-1)-\eta_s e-b}{ce}\right]\eta_n-\left[\eta_s^3+\frac{d(\eta_s e+b)}{ce}\right]=0 \tag{25a}$$

$$\xi_n = \xi_s - (\eta_n - \eta_s)\cot\phi_s \tag{25b}$$

where

$$b = \xi_s\sin 2\phi_s - \eta_s\cos 2\phi_s$$

$$c = 1/(2\xi_s\sin 2\phi_s)$$

$$d = \xi_s\tan\phi_s - \eta_s$$

$$e = (1/\lambda_n)\left(2\sin\alpha\cos\theta_s-\left|\sum_{j=1}^{n-1}w_j'\right|\right)$$

Equation (25a) has one real root; the other two complex conjugate roots are disregarded.

The position of this vortex pair at the subsequent axial station $x_n + \Delta x$, together with the other discrete pairs previously shed, is computed by evaluating the total velocity induced at the vortices. For the generic right side discrete vortex, it is

$$(\xi_j)_{x_n+\Delta x} = (\xi_j)_{x_n} + (u')_{x_n}\Delta x \tag{26a}$$

$$(\eta_j)_{x_n+\Delta x} = (\eta_j)_{x_n} + (v')_{x_n}\Delta_x \tag{26b}$$

where u' and v' represent the components along the ξ and η axes of the total velocity induced at $\sigma = \sigma_j$; they contain the contributions of the growing body velocity, the crossflow velocity and the velocity induced by all n discrete vortex pairs plus their images, except for the contribution of the jth vortex itself.

Normal Force Distribution

The total impulse to a unit length of a two-dimensional cylinder of a pair of vortices of equal and opposite strength Γ_j is[6]

$$I_j = i\rho\Gamma_j(\sigma_j - r_0^2/\bar{\sigma}_j + \bar{\sigma}_j - r_0^2/\sigma_j) \tag{27}$$

where r_0 is the cylinder radius and $\sigma_j, -\bar{\sigma}_j$, the position of the vortex pair. Within the assumptions of slender-body theory, the normal force on a length Δx of the body in the presence of n discrete vortex pairs is given by

$$\Delta N = V_\infty \cos\alpha \left\{\sum_{j=1}^{n} \Delta I_j\right\} \tag{28}$$

where ΔI_j represents the variation of the impulse I_j between x and $x + \Delta x$. Since the initial value of I_j at the body nose is zero, the total normal force at the station x_n is simply given by Eq. (28) when I_j is substituted by the value of the impulse evaluated at x_n. Similarly, for $n - 1$ discrete vortex pairs and a vortex sheet pair, the normal force coefficient due to vortex separation is found to be

$$(C_{N_v})_{x_n} = \frac{8\cos\alpha}{a}\sum_{j=1}^{n-1}\lambda_j'[(\xi_1)_j - (\xi_2)_j]_{x_n} + \frac{2kr_0^4\cos\alpha}{\pi a^2 V_\infty}\left\{\frac{1}{3}\bar{r}_A^4\cos\theta_s\cos(\phi_s - \theta_s) + \sum_{m=5}^{\infty}(-1)^m\frac{2\bar{r}_A^m}{m(m-1)}\cos[(m-3)\phi_s - (m-2)\theta_s]\right\} \tag{29}$$

where

$$(\xi_1)_j = |\sigma_j|\cos\theta_j$$

$$(\xi_2)_j = (\xi_1)_j r_0^2/|\sigma_j|^2$$

$$\lambda' = \lambda r_0/a$$

The coefficient of local normal force, C_{n_x}, and of pitching moment, C_{m_v}, induced by vortex separation are then given by

$$C_{n_x} = (dC_{N_v}/dx)_x \tag{30a}$$

$$C_{m_{v_x}} = \frac{1}{2a}\int_0^x C_{n_x}\,dx \tag{30b}$$

The local normal force or normal force per unit length on the three-dimensional inclined body is the same as the cross-flow drag on the two-dimensional cylinder, which can be obtained directly from Eq. (27), being $D = dI/dt$.

5. Initial Conditions and Step Size

The starting process of Ref. 7 can be incorporated into the present work. An initial vortex strength is, however, not necessary to start the computation. In fact, because of the use of the finite difference technique the computation can start at an arbitrary point, close to the body apex and where the initial vortex strength is zero, and proceed along the body until a nontrivial value is obtained. This criterion is equivalent to the one obtained analytically in Ref. 7.

The development of the vortex sheet consists of following the positions of a set of free vortices as they progress along the body. These positions are evaluated using a step-by-step computation of the velocities that the vortices mutually induce.

The choice of the step size determines the number of vortices being used to approximate the actual continuous vortex sheet and influences the accuracy of the computation of the vortex trajectory. Theoretically, the accuracy of the method should improve as the number of vortices introduced becomes larger. However, the distribution of vortices inside the external vortex spiral becomes more irregular as the number of vortices increases. This distortion seems to be produced mainly by round-off and truncation errors in the calculation of the vortex positions. Use of a step size smaller than the one at which a new pair of vortices is introduced may not prevent this distortion but may produce higher cumulative numerical errors.

In order to minimize the sensitivity of the vortex trajectory, and consequently of the induced forces, to the step size, the induced velocities at the vortices can be evaluated as an average of their values computed at the upstream and downstream edge of each step. In so doing, a larger step size can be used and consequently the number of vortices can be reduced. The average procedure will also increase the accuracy of the Kutta condition which is satisfied only at discrete axial stations.

Exploratory calculations conducted on slender cones at various angles of attack have shown that the first vortex spiral can be successfully represented with 15 to 20 vortices of approximately equal strength, that is, within 15 to 20 steps. The subsequent internal spirals start to show significant irregularity when more than 30 to 40 vortices have been shed. In order to decrease the vortex accumulation inside the external spiral, the step size was increased assuming a linear variation with the body radius. The external spiral was not influenced by the variation of step size, and the center of vorticity remained practically constant. The computing time, which increases exponentially with the number of vortices being used, was drastically reduced. The variation of the step size with the body radius affords the advantage of using small step size only when most needed, that is, at the beginning of the vortex sheet development.

For cones, the relationship among number of vortices n, body slenderness l/d, and initial step size Δx_0 can be represented as follows:

$$\frac{l}{d} = \left(\frac{x_s}{d}\right)(1+R)^n + \left(\frac{\Delta x_0}{d}\right)\left[1 + \sum_{m=1}^{n-1}(1+R)^m\right] \tag{31}$$

where R is the step increment control parameter such that

$$x_i = x_{i-1} + [\Delta x_0 + (R/\tan\epsilon)r_0 x_{i-1}], \quad R = \text{const} \tag{32}$$

and x_s is the axial point of separation. Equation (31) solved in terms of n becomes

$$n = \frac{1}{ln(1+R)}\,ln\left[\frac{\Delta x_0 + 2R(l/d)}{\Delta x_0 + 2R(x_s/d)}\right] \tag{33}$$

The values of Δx_0 and R are chosen in order that the length of the elementary vortex sheet lies well within the approximations of the theory (Sec. 4). This is satisfactorily accomplished when $\bar{r}_A$ is less than $\frac{1}{10}$ of the local radius. It should be noted that the vortex of substitution is placed at $\frac{1}{3}$ of such a length. For slender bodies other than cones, Eq. (33) can still be used as an approximate value when an "equivalent" cone is substituted for the actual configuration.

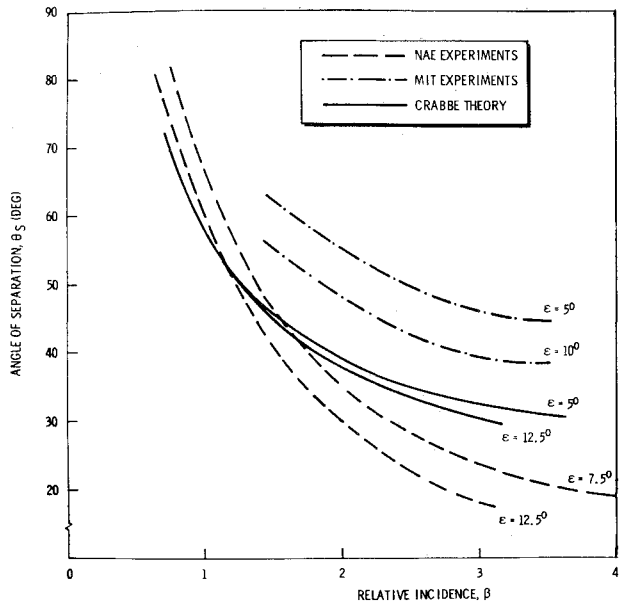

Fig. 2 Angle of separation for circular cones.

6. Separation Points

The viscous inputs of the present analysis are the separation point coordinates (x_s, θ_s) which are a function of the body geometry, angle-of-attack and freestream conditions. Reliable, systematic data on the separation points are available only for a few configurations. These data are often restricted to a limited Reynolds and Mach number range.

The configurations most often investigated are slender cones under both laminar and turbulent separation conditions.[2,3,15] The most significant results of such investigations are summarized here. Both for laminar and for turbulent separation, the axial point of separation x_s is located at the cone tip; incipient vortex separation starts at a relative incidence β of about 0.8, although no appreciable vortex effects are experienced until $\beta \cong 1.0$ to 1.1. The cross-flow point of separation θ_s is a function of relative incidence, as shown in Fig. 2; the figure reports the results of the tests conducted at MIT and NAE on slender cones under laminar boundary-layer separation and the results of Crabbe's theory.[16] For turbulent separation, the results of previous investigations[17] indicated the angle of separation to be constant with relative incidence. However, the results of Rainbird's recent tests on a 12.5° cone under turbulent boundary-layer separation have indicated that the separation angle is a function of relative incidence, and that the flow features were "qualitatively similar" to laminar boundary-layer separation at low speeds.[15] The differences between the results of Refs. 16 and 17 may be in part explained by the use of different criteria assumed in the definition of the separation angle. Further details are discussed in Ref. 14.

For nonconical axisymmetric bodies where sensible three-dimensional effects are present, the definition of the separation points requires the use of semiempirical criteria based on the cone analogy. Such criteria are discussed in some detail in Refs. 7 and 8.

7. Results and Discussion

Several axisymmetric configurations have been analyzed using the MDAC-W CDC 6500 computer. A plotting subroutine was included in the computer program in order to depict graphically the development of the vortex sheet as it proceeds along the body axis. The results of some of these computations are reported in Figs. 3–7. Figure 3 shows the development of the vortex sheet at the beginning of the computation for a 7.8° semiapex cone at a relative incidence β = 1.95. After the tenth step, the discrete vortices have completed the first spiral; in the subsequent steps (top left of Fig. 3) the vortices continue to roll up about the sheet center of gravity which maintains a constant relative location. The number of vortices used in this case was 64; the step size, starting from a value equal to 1.67% of the base radius, was increased linearly with the local radius of the cone. This step size variation was used to reduce the computing time and the sensitivity of the vortex trajectory (and consequently of the normal forces) to a constant step size. In fact, no significant variation of circulation strength and induced normal force has been noticed using different numbers of vortices (Fig. 9 of Ref. 14).

The correlation for the total vortex strength is evident from Fig. 4; the small differences of the order of 5 to 10% depending on relative incidence are due mostly to different

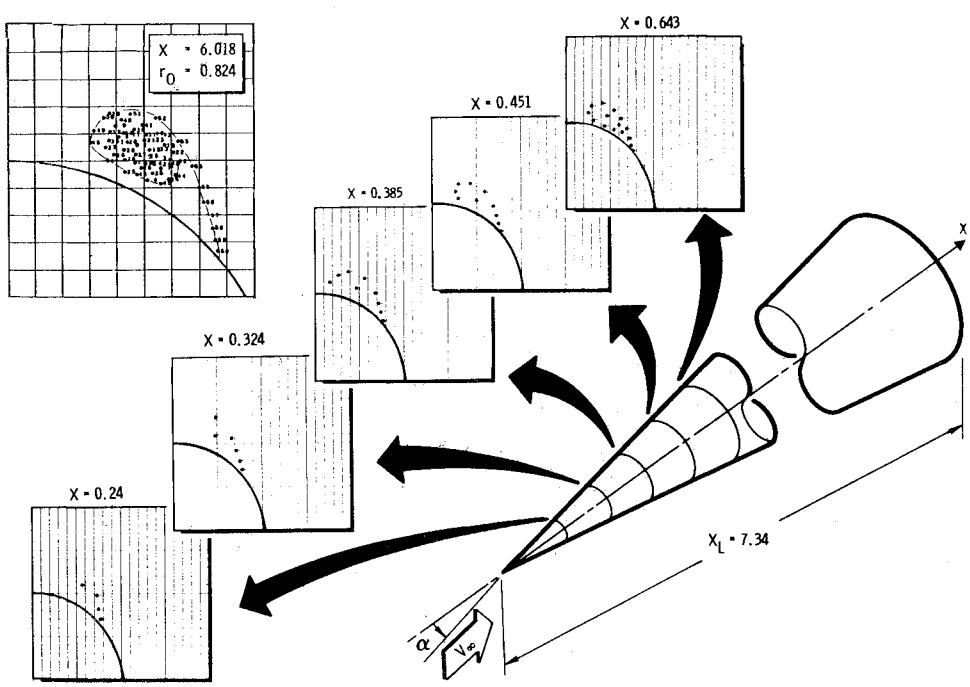

Fig. 3 Development of the vortex sheet spiral for β = 1.95.

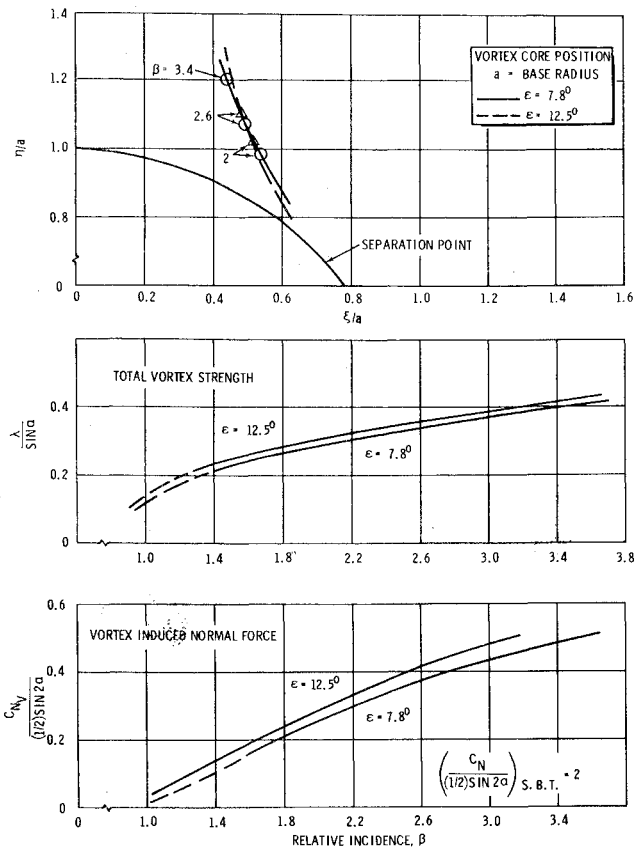

Fig. 4 Correlation curves for circular cones using $\theta_s = 40°$.

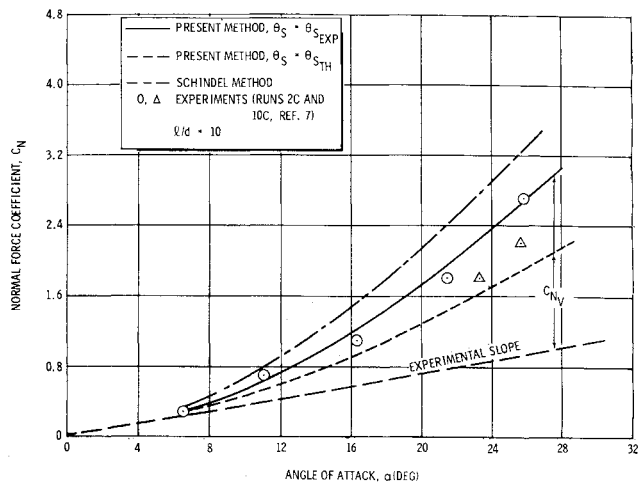

Fig. 6 Normal force coefficient of blunted ogive-cylinder configuration.

error accumulation in the computation (different numbers of vortices were used). The induced normal force which is a function of both vortex strength and position, shows larger percentage differences. For both cones, the effects of flow separation become appreciable when $\beta \geq 1.1$ in good agreement with experimental data.[2,3,15] At lower values of β an irregular vortex sheet develops remaining very close to the body surface and resembling a vortex bubble more than a vortex sheet.

In Fig. 5a, the vortex sheet developed by a 12.5° cone under laminar boundary-layer separation is compared with the positions of the primary, secondary, and tertiary vortices as measured by Rainbird et al.[2] The experimental center of vorticity has been estimated from the strength of the vortices,

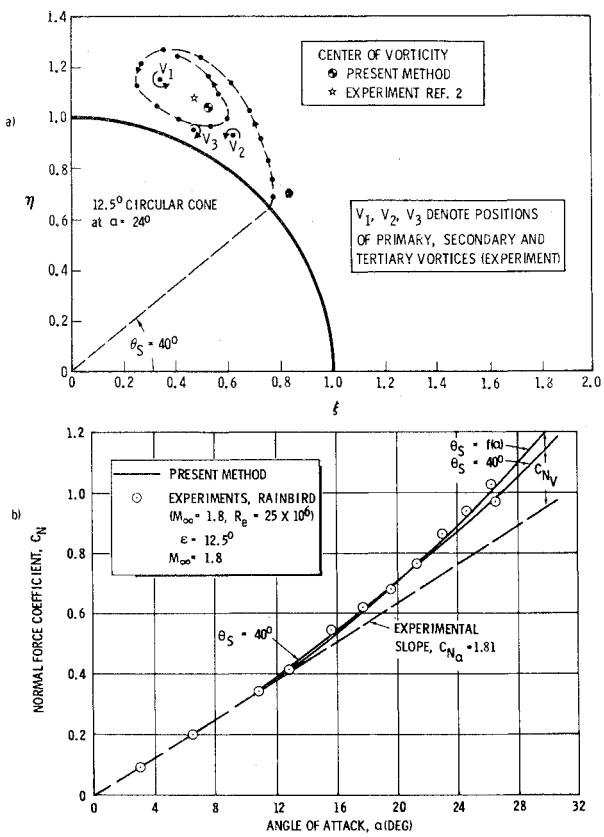

Fig. 5 Vortex sheet and normal force coefficient of 12.5° circular cone.

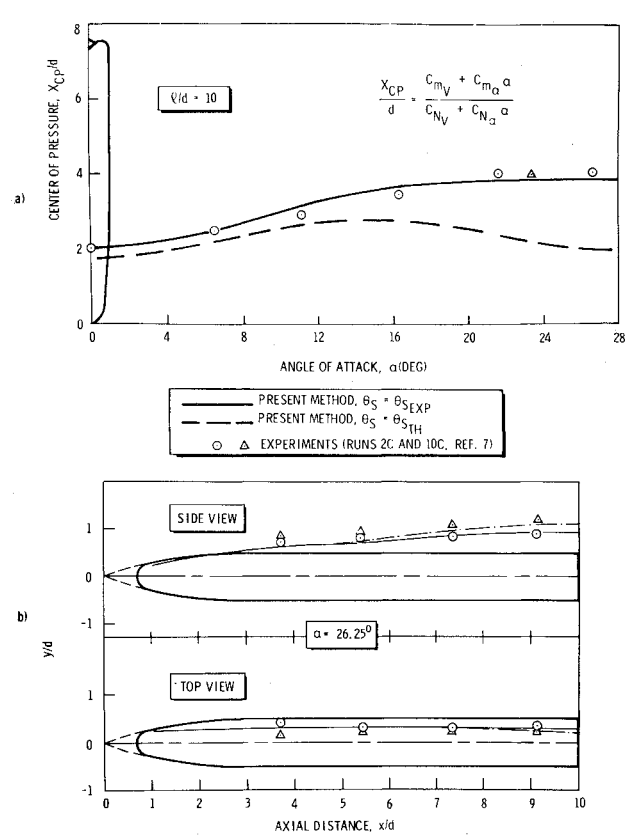

Fig. 7 Center of pressure variation and vortex core trajectory.

evaluated by Rainbird in Ref. 2, at an intermediate axial station $x/l = 0.4$.

The normal force induced by vortex separation on a 12.5° circular cone under turbulent boundary-layer separation is presented in Fig. 5b. The total normal force has been evaluated under the assumptions expressed by Eq. (1). The curve corresponding to the $\theta_s = 40°$ angle, shows good agreement with experiments up to $\alpha \cong 22°$ while underestimating the induced normal force at higher angles of attack. The induced normal force has been also evaluated using as angle of separation the function $\theta_s = f(\beta)$ of Fig. 2, which represents the results of Crabbe's theory for circular cones under laminar separation. This assumption is supported by large flowfield similarities of the laminar and turbulent boundary-layer separation of circular cones, as observed by Rainbird;[15] the agreement, especially at higher angles of attack, is more satisfactory than the $\theta_s = \text{const}$ case. For circular cones, more calculations and comparisons with experimental data can be found in Ref. 14.

Finally, a blunted-nose tangent-ogive cylinder combination of slenderness ratio $l/d = 10$ has been analyzed under laminar vortex separation. The results of the calculation of induced normal forces, center of pressure, and vortex core trajectories are reported in Figs. 6 and 7; the experimental results of Schindel and Chamberlain[7] have been included for comparison. The angle of separation has been assumed to be a function of axial distance; both the experimental and theoretical variation of Ref. 7 have been considered. In particular the experimental $\theta_s(x)$ assumed here is an average of the two functions reported in Fig. 53 of Ref. 7. Vortex separation is assumed to start at the ogive-cylinder junction for low angles of attack moving towards the nose tip ($x_s \cong 1.85a$) as the angle of attack increases, according to the experimental data of Ref. 7. In Fig. 6 the total normal force has been evaluated adding the calculated vortex induced normal force to the linear value estimated from the initial slope of the experimental curve. Also included are Schindel's theoretical results for laminar separation, presumably obtained using the same theoretical angle of separation, $\theta_{s_{th}}$. In Fig. 7a experimental slopes were used to evaluate C_{m_α} and C_{N_α} for the $\theta_s = \theta_{s_{exp}}$ case while theoretical values were estimated for the $\theta_s = \theta_{s_{th}}$ case. The curves of the Figs. 6 and 7 show satisfactory agreement with the experimental data when $\theta_{s_{exp}}$ is used as an input; with the theoretical separation angles of Ref. 7, both normal force and center of pressure are underestimated, especially at large angles of attack.

8. Conclusions

The primary advantages of the present method can be summarized as follows: 1) The actual vortex sheets are realistically represented by a finite number of discrete free vortices. 2) The computing time is not a function of the body configuration but of the number of vortices used to represent the vortex sheets. This allows, within convergence limits, control of the accuracy of a given computation. 3) The method is applicable to any slender axisymmetric body. 4) The governing equations are solved in closed form at each axial position without use of iterative procedures.

The accuracy to which the vortex core, vortex strength, and normal force are evaluated depends on the accuracy of the viscous inputs, that is, of the points of separation. From the results reported in the previous section and in particular from those configurations for which reliable experimental data were available, it can be concluded that the accuracy of the method is more than satisfactory. The use of Eq. (1) for the evaluation of the total normal force has extended the range of applicability of this and similar theories. In fact, while the vortex induced forces are evaluated from a solution of the Laplace equation, the linear force due to the attached flow can be evaluated using the best available linearized theory or experimental data. In addition, experiments have shown that the vortical lift is almost independent of Mach number in a broader velocity range than that allowed by the slender body theory assumptions. This is confirmed by the satisfactory results obtained on slender cones up to $M_\infty \cong 2$.

The present multivortex model can be used to evaluate vortex separation effects on configurations of asymmetrical cross section. Its applicability will be limited to configurations for which conformal mapping functions can be evaluated and separation data are available or known "a priori." The latter case includes, in addition to the well known case of a wing exhibiting leading edge separation, all configurations having sharp corners or cross section discontinuities.

References

[1] Rainbird, W. J., Crabbe, R. S., Peake, D. J., and Meyer, R. R., "Some Examples of Separation in Three-Dimensional Flows," *Canadian Aeronautics and Space Journal*, Dec. 1966, pp. 409–423.

[2] Rainbird, W. J., Crabbe, R. S., and Jurewicz, L. S., "A Water Tunnel Investigation of the Flow Separation About Circular Cones at Incidence," Aero Rept. LR-385, Sept. 1963, National Research Council of Canada, Ottawa, Canada.

[3] Friberg, E. G., "Measurement of Vortex Separation: Part II—Three-Dimensional Circular and Elliptic Bodies," TR 115, Aug. 1965, MIT Aerophysics Lab., Cambridge, Mass.

[4] Edwards, R. H., "Leading Edge Separation From Delta Wings," *Journal of Aeronautical Sciences*, Vol. 21, 1954, p. 134.

[5] Brown, C. E., and Michael, W. H., "On Slender Delta Wings With Leading-Edge Separation," TN 3430, April 1955, NACA.

[6] Bryson, A. E., "Symmetric Vortex Separation on Circular Cylinders and Cones," *Journal of Applied Mechanics*, Dec. 1959, pp. 643–648.

[7] Schindel, L. H., and Chamberlain, T. E., "Vortex Separation on Slender Bodies of Elliptic Cross Section," TR 138, Aug. 1967, MIT Aerophysics Lab., Cambridge, Mass.

[8] Schindel, L. H., "Effects of Vortex Separation on the Lift Distribution on Bodies of Elliptic Cross Section," *Journal of Aircraft*, Vol. 6, No. 6, Nov.-Dec. 1969, pp. 537–543; also Rept. TR 118, Sept. 1965, MIT.

[9] Mangler, K. W., and Smith, J. H. B., "Calculation of the Flow Past Slender Delta Wings With Leading Edge Separation," Rept. Aero. 2593, May 1957, Royal Aircraft Establishment, Farnborough, England.

[10] Smith, J. H. B., "Improved Calculations of Leading-Edge Separation From Slender Delta Wings," TR 66070, March 1966, Royal Aircraft Establishment, Farnborough, England.

[11] Sacks, A. H., Lundberg, R. E., and Hanson, C. W., "A Theoretical Investigation of the Aerodynamics of Slender Wing-Body Combinations Exhibiting Leading-Edge Separation," CR 719, March 1967, NASA.

[12] Schindel, L. H., "Separated Flow About Lifting Bodies," TR 80, Sept. 1963, MIT Aerophysics Lab., Cambridge, Mass.

[13] Kuchemann, D., "Types of Flow on Swept Wings," *Journal of the Royal Aeronautical Society*, Vol. 57, Nov. 1953, pp. 683–699.

[14] Angelucci, S. B., "A Multivortex Method for Evaluating Vortex-Induced Forces on Axisymmetric Bodies at Angle of Attack," MDC G0613, June 1970, McDonnell-Douglas Astronautics Co., Huntington Beach, Calif.

[15] Rainbird, W. J., "Turbulent Boundary Layer Growth and Separation on Yawed Cone," *AIAA Journal*, Vol. 6, No. 12, Dec. 1968, pp. 2410–2416.

[16] Crabbe, R. S., "Flow Separation About Elliptic Cones at Incidence," AIAA Paper 65-396, July 1965, San Francisco, Calif.

[17] Jorgensen, L. H., "Elliptic Cones Alone and With Wings at Supersonic Speeds," TN 4045, Oct. 1957, NACA.